JCTA Journal of Computing Theories and Applications ISSN:3024-9104

Research Article

A Cubical Persistent Homology-Based Technique for Image Denoising with Topological Feature Preservation

Md. Al-Imran *, Mst Zinia Afroz Liza, Md. Morshed Bin Shiraj, Md. Masum Murshed and Nasima Akhter

Department of Mathematics, University of Rajshahi, Rajshahi-6205, Bangladesh;
email: zmimran001@gmail.com; ziniaafroz913@gmail.com; mbshiraj@gmail.com;
mmmurshed82@gmail.com; nasima.math.ru@gmail.com
* Corresponding Author : Md. Al-Imran

Abstract: Image denoising is a fundamental challenge in image processing, where the objective is to remove noise while preserving critical image features. Traditional denoising methods, such as Wavelet, Total Variation (TV) minimization, and Non-Local Means (NLM), often struggle to maintain the topological integrity of image features, leading to the loss of essential structures. This study proposes a Cubical Persistent Homology-Based Technique (CPHBT) that leverages persistence barcodes to identify significant topological features and reduce noise. The method selects filtration levels that preserve important features like loops and connected components. Applied to digit images, our method demonstrates superior performance, achieving a Peak Signal-to-Noise Ratio (PSNR) of 46.88 and a Structural Similarity Index Measure (SSIM) of 0.99, outperforming TV (PSNR: 21.52, SSIM: 0.9812) and NLM (PSNR: 22.09, SSIM: 0.9822). These results confirm that cubical persistent homology offers an effective solution for image denoising by balancing noise reduction and preserving critical topological features, thus enhancing overall image quality.

Keywords: Cubical Complex; Image Analysis; Persistent Homology; Sublevel Set Filtration; Topological Data Analysis.

1. Introduction

Image denoising is a fundamental challenge in image processing, aiming to remove noise while preserving critical image features. Traditional denoising methods, such as wavelet-based techniques [1], total variation (TV) minimization [2], and non-local means (NLM) algorithms [3], wavelet transforms [4], have been widely adopted. However, these methods present certain limitations that impact their ability to maintain the topological integrity of image features, which is crucial for many applications. Wavelet Transforms efficiently reduce noise by decomposing an image into different frequency components. However, they are highly sensitive to threshold selection, and improper thresholding can lead to the loss of significant topological details, such as small loops and fine structures [1].

Additionally, wavelet-based methods assume smoothness, which makes them less effective for preserving complex or non-smooth structures in the data [4]. TV Minimization is known for its ability to preserve edges but often over smooth textures, leading to the loss of fine topological features [2]. Moreover, the success of TV minimization heavily depends on the choice of the regularization parameter, which can be difficult to tune correctly. Higher values can result in excessive smoothing, while lower values may not effectively reduce noise [5]. NLM Algorithms excel in texture preservation by comparing image patches, but they struggle to maintain global topological structures, which may result in the loss of significant features, particularly in images where the noise pattern is complex or non-repetitive [3]. Furthermore, NLM is computationally expensive and relies heavily on selecting appropriate patch sizes, making it less practical for large datasets [6].

These limitations complicate extracting meaningful topological features from noisy data, particularly in images found in the digit dataset, where both local textures and global topological structures are essential for proper image analysis. In many cases, conventional methods

Received: September, 9th 2024
Revised: September, 28th 2024
Accepted: October, 5th 2024
Published: October, 6th 2024

fail to adequately balance noise reduction with preserving significant features, leading to suboptimal results in downstream analysis tasks.

Conventional denoising techniques, including median filtering [7] and sparse representation methods [8], have been extensively studied and applied across various contexts. These methods typically rely on local pixel information, making them effective in certain scenarios.

Recent research has explored various applications of persistent homology in image denoising. One approach combines persistent homology with deep residual learning for three-dimensional block-matching denoising, demonstrating improved effectiveness in removing Gaussian noise [9]. A novel topological loss function based on persistent homology has been proposed for low-light image denoising, specifically addressing the challenges posed by spatially variant noise characteristics [10]. This method operates in the space of image patches, calculating topological invariants represented by persistence diagrams, thereby offering robust resistance to noise across multiple scales. In [11], the authors utilized cubical homology to efficiently extract topological features in image classification, combining it with machine learning for improved accuracy. Researchers in [12] proposed a preprocessing algorithm to recover topological information lost in noisy datasets, while the authors of [13] developed a multi-parameter persistence framework for image denoising using mathematical morphology, achieving results comparable to deep learning methods.

In contrast to these conventional approaches, persistent homology offers a global perspective for denoising, capturing topological features that persist across different scales, making it a promising tool for robust denoising [14]. Persistent homology has gained attention in recent years for its ability to capture the underlying structure of data, particularly in image processing, where preserving topological features such as edges, loops, and voids is crucial. Unlike traditional methods that may compromise global data structures, persistent homology provides a framework for analyzing data across multiple scales, preserving the most significant topological features while filtering out noise.

Cubical persistent homology, which operates on cubical complexes, is especially advantageous for image data, which is naturally represented as a grid of pixels. This approach constructs a sequence of nested cubical complexes, each representing the image at a different scale, and tracks the appearance and disappearance of topological features across these scales. The persistence of these features is recorded in a persistence diagram, where those with longer lifetimes are deemed more significant and less likely to be noise [15]. This global perspective allows for a more accurate distinction between noise and meaningful features, a limitation of traditional denoising methods.

The foundations of persistent homology were established in [16], and [17], where the utility of this approach for analyzing simplicial complexes was demonstrated. However, these methods were not optimized for cubical complexes, which are better suited for image data. In [18], the authors addressed this gap by demonstrating the computational efficiency of cubical complexes for image analysis. Their work paved the way for the application of cubical persistent homology in image denoising, particularly for datasets like Fashion-MNIST, where maintaining the integrity of topological features is crucial. While persistent homology has been computed using cubical complexes in studies such as [19], [20], and [21], none of these works have specifically applied this approach to image denoising.

Despite the potential of persistent homology, its use in image denoising remains relatively unexplored, with most research focusing on feature extraction and shape analysis [22] rather than noise reduction. Recent work in [15] provided a comprehensive review of persistent homology applications, including cubical complexes, which demonstrated the effectiveness of these methods in noisy data environments. The use of persistent homology for image denoising, focusing on extracting robust topological features, was explored in [23]. In [24], the utility of persistent homology for feature extraction from noisy data was demonstrated, but the method did not fully exploit the advantages of cubical complexes. The authors in [25] examined the computational aspects of persistent homology but did not focus on its application to image denoising. Similarly, in [26], the use of persistent homology in analyzing noisy data was explored, but without providing a comprehensive methodology for filtration level selection. However, selecting an appropriate filtration level, the scale at which topological features are considered significant presents a complex challenge. This filtration level is crucial as it determines which features are preserved and removed as noise [24]. Current research often underestimates the complexity of choosing this threshold, especially in high-dimensional data where interactions between topological features are intricate and non-linear [27].

In [28], the researchers denoised images by removing unnecessary rows and columns and binarizing them during the preprocessing step to train hardware-embedded graphical models. However, they did not consider the significant topological features of the images during the binarization process. The absence of a systematic approach to selecting filtration levels has led to inconsistent results in previous studies, where either excessive noise is retained, or essential topological features are lost.

Further contributions and objectives of this research are:

- Propose a new method for selecting optimal filtration levels in persistent homology.
- Highlight the limitations of traditional denoising techniques and show how persistent homology overcomes these issues.
- Demonstrate that the method preserves key topological features like loops and connected components while reducing noise.
- Compare the method to existing techniques, showing superior PSNR and SSIM metrics results.
- Introduce a robust framework for noise reduction in noisy data environments, maintaining critical topological information.

This paper is structured as follows: Section 2 details the mathematical background necessary for understanding cubical complexes and persistent homology. Section 3 introduces the proposed methodology, including the filtration level selection and denoising techniques. Section 4 presents experimental results, demonstrating the efficacy of our approach on the digit dataset. Finally, Section 5 concludes the paper with a discussion of the implications of our findings and potential avenues for future research.

2. Preliminaries

2.1. Persistent Homology

Definition: The α-sublevel set of a function $f: \mathbb{R}^n \to \mathbb{R}$ is the set $L_\alpha^{-1}(f) = \{x \in \mathbb{R}^n \mid f(x) \leq \alpha\}$. The sublevel sets are of the form $f^{-1}\big((-\infty, \alpha]\big)$. In Fig. 1, we have the α-sublevel set $f: \mathbb{R}^2 \to \mathbb{R}$.

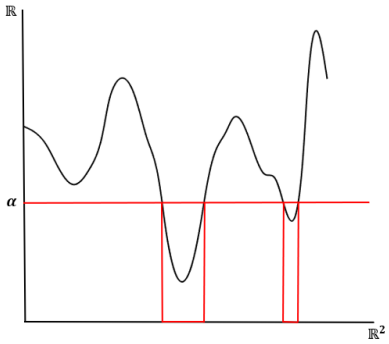

Figure 1. Example of sublevel set.

Let X be a simplicial (cubical) complex. A function $f: \Sigma(X) \to \mathbb{R}$ on the simplices (cubes) of X is a monotonic map if it maps each simplex (cube) to a value in $\mathbb{R}$ in such a way that if τ is a face of σ, then $f(\tau) \leq f(\sigma)$. Given such a map f, the sublevel set filtration of f is the collection of simplicial (cubical) complexes, as in Equation (1), along with inclusion maps, in Equation (2)

$$\{f^{-1}(-\infty, \alpha] \mid \alpha \in \mathbb{R}\} \tag{1}$$

$$f^{-1}(-\infty, \alpha'] \subseteq f^{-1}(-\infty, \alpha] \tag{2}$$

Here f is known as a filter, and α is the filtration index; for all $\alpha' \leq \alpha \in \mathbb{R}$.

While dealing with data, standard topological quantities might be very susceptible to noise as well as small geometric changes; persistent homology solves this issue by looking at a collection of spaces that are modeled by a cubical complex X with a filter function $f: X \to$

$\mathbb{R}$ defining to each cell the scale that defines where this cube appears; these spaces are indexed by a real variable that typically represents the growing length scale.

Definition [29]: From a filtered complex X, we derive inclusions of sub-level sets where $\alpha' \leq \alpha$ as follows: $f^{-1}(-\infty, \alpha'] \hookrightarrow f^{-1}(-\infty, \alpha]$. These inclusions produce linear transform between vector spaces, see Equation (3).

$$H_k(f^{-1}(-\infty, \alpha']) \hookrightarrow H_k(f^{-1}(-\infty, \alpha]) \tag{3}$$

when degree-k homology with coefficients in $\frac{\mathbb{Z}}{2\mathbb{Z}}$ is applied. The functor $H_k(f): (\mathbb{R}, \leq) \rightarrow Vec_{\mathbb{Z}/2\mathbb{Z}}$ that results from the post category $(\mathbb{R}, \leq)$ to the category of vector spaces over the field $\frac{\mathbb{Z}}{2\mathbb{Z}}$ is referred to as a persistence module. For more information, see [27].

As mentioned in [27], Gabriel's Theorem from representation theory suggests that the persistence module $H_k(f)$ can be expressed as a combination of persistence modules consisting of $\frac{\mathbb{Z}}{2\mathbb{Z}}$ for α values within the interval $[b, d)$, linked by identity maps, and being 0 elsewhere. These modules are termed as interval modules $\mathbb{I}_{[b,d)}$: $H_k(f) \cong \bigoplus_{l \in L} \mathbb{I}_{[b_l, d_l]}$.

Each interval component $\mathbb{I}_{[b_l, d_l]}$ signifies a degree-k homological feature that is born at $\alpha = b_l$ and vanishes at $\alpha = d_l$. In cases where the final space X exhibits non-trivial homology, features persist indefinitely. These features have $d_l = \infty$, and the corresponding interval is referred to as essential. The degree-k persistence diagram of f is the multiset, see Equation (4).

$$Dgm^k(f) = \{[b_l, d_l) | l \in L\}. \tag{4}$$

We write $[b_l, d_l)_k \in Dgm^k(f)$ to denote the homological degree of an interval and define the persistence diagram of f as the disjoint union overall degrees, see Equation (5).

$$Dgm(f) = \bigcup_{k=0}^{\dim(X)} Dgm^k(f). \tag{5}$$

Writing $Dgm_F(f)$ for the multiset of finite intervals with $d_l < \infty$, and $Dgm_\infty(f)$ for the remaining essential ones, we obtain $Dgm(f) = Dgm_F(f) \cup Dgm_\infty(f)$.

In persistent homology, several key topological variables, as shown in Table 1, define the structure and significance of features in an image. These variables are critical in distinguishing noise from important structures during image analysis.

Table 1. Topological variables related to persistent homology.

Variable	Description	Determination
Birth Time	The filtration value (or pixel intensity threshold) at which a topological feature appears.	Represents when a feature begins to emerge in the image.
Death Time	The filtration value at which a topological feature disappears, indicating that it has merged with another feature or has been filled in.	Represents when a feature becomes irrelevant or absorbed.
Persistence Diagram	A diagram plotting the birth and death of topological features across different filtration levels, providing a comprehensive overview of significant features.	Used to visualize the lifetime and importance of each feature in a concise form.
Persistent Barcode	A visual representation of the persistence of features, where longer bars correspond to more significant features.	Helps to identify which topological features persist across multiple scales, distinguishing noise from critical structures.
Dimension	Topological dimension: 0 represents connected components, and 1 represents loops. Higher-dimensional features can also be captured, but this work focuses on dimensions 0 and 1.	Determined automatically by computing cubical homology on the image.

2.2 Filtration of Cubical Complex

Definition: A set of n-cubes in $\mathbb{R}^m$ such that $0 \leq n \leq m$, and that every face of a cube in $\mathcal{K}$ is also in $\mathcal{K}$. The intersection of any two cubes of $\mathcal{K}$ is either empty or a common face, is called a cubical complex.

Through a nested sequence of subspaces or filtration, persistent homology [16], [17] facilitates us to calculate the topological properties of a space by providing a persistence diagram that shows the connected components, loops, and voids that arise and disappear as we move through the filtration. Digital images are among the many situations in which it finds utility, such as the research of porous materials [30], hurricanes [31], or medical applications [32]. While simplicial complexes resulting from point clouds are commonly dealt with persistent homology, since digital images consist of pixels (in dimension $m = 2$) or voxels (for $m \geq 2$), cubical complexes are the obvious choice because they mirror the regular grid of numbers used to store the image.

From an image $\mathcal{I}$, a cubical complex can be created in two different ways: Voxels are represented by vertices in the V-construction $V(\mathcal{I})$ and by lines in the T-construction Top-dimensional cubes are used by $T(\mathcal{I})$ to represent voxels. These constructions bear a striking resemblance to two distinct voxel connectivities found in classical digital topology. The V-construction is consistent with what is referred to as "direct connectivity" in computer science, in which each voxel has $2m$ neighbors if and only if its grid coordinates differ by one. Pixels with $m = 2$ are 4-connected, and the closest neighbors are on the left and right, as well as above and below. The T-construction corresponds to indirect connectivity, where voxels are also connected diagonally, every voxel has $3^m - 1$ neighbors and pixels are 8-connected.

The fact that the persistent homology can differ significantly when calculated using the V and T-constructions for the same image should come as no surprise; (see Fig. 6 and 10) illustrates an example. Interior vertices of the T-construction correlate top-cells in the V-construction, and vertices in the V-construction relate to top-dimensional cells in the T-construction.

Definition [29]: A grayscale digital image with m-dimensions $(p_1, p_2, \cdots, p_m)$is represented as a $\mathbb{R}$-valued array $\mathcal{I} \in N_{p_1 \times p_2 \times \cdots \times p_m}(\mathbb{R})$. On an m-dimensional rectangular grid $\mathcal{I}$, it can be expressed equivalently as Equation (6).

$$\mathcal{I}: E = [\![1, p_1]\!] \times [\![1, p_2]\!] \times \cdots \times [\![1, p_m]\!] \to \mathbb{R}, \tag{6}$$

Where $[\![1, p_i]\!]$ represents the set $\{ n \in \mathbb{N} \mid 1 \leq n \leq p_i \}$. The image domain is another term for the index set, E, of $\mathcal{I}$ (Fig. 2). Take note of that when $m = 2$, elements $q \in E$ are termed pixels, and if $m \geq 3$, they are defined as voxels. The grayscale value of q is represented by the value $\mathcal{I}(q) \in \mathbb{R}$.

The canonical topology on $E \subseteq \mathbb{Z}^m \subset \mathbb{R}^m$ makes it a completely disconnected discrete space, making it difficult to analyze such images via their sub-level sets using persistent homology. Regular cubical complexes model grayscale digital images to infer a meaningful topology on the image, which more accurately stands for the perceived connectivity of the voxels [33].

Building a filtered cubical complex from an image $\mathcal{I}: E \to \mathbb{R}$ can be done in two popular ways. As demonstrated in [30], one approach involves representing the voxels as the cubical complex's vertices. This cubical complex is known as vertex construction or simply V-construction. The second approach, known as top-cell construction, or T-construction, treats voxels as top-dimensional cells. As stated in [33], the top-cell structure matches the indirect adjacency model, while the vertex construction correlates to the graph-theoretical direct adjacency utilized in conventional digital image processing. Additionally, these adjacent models are known as the open as well as closed digital topologies, respectively. Fig. 2 shows a digit image and its corresponding pixel values as an array.

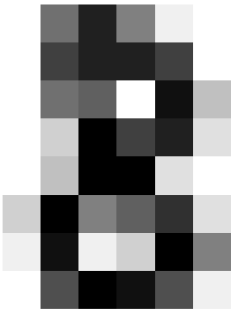

$$\begin{pmatrix} 16 & 16 & 7 & 2 & 8 & 15 & 16 & 16 \\ 16 & 16 & 4 & 2 & 2 & 4 & 16 & 16 \\ 16 & 16 & 7 & 6 & 16 & 1 & 12 & 16 \\ 16 & 16 & 13 & 0 & 4 & 2 & 14 & 16 \\ 16 & 16 & 12 & 0 & 0 & 14 & 16 & 16 \\ 16 & 13 & 0 & 8 & 6 & 3 & 14 & 16 \\ 16 & 15 & 1 & 15 & 13 & 0 & 8 & 16 \\ 16 & 16 & 5 & 0 & 1 & 5 & 15 & 16 \end{pmatrix}$$

(a) (b)

Figure 2. Image of (**a**) Digit 8 and; (**b** its array.

The process of extracting the V-construction from an image is illustrated in Figs. 3 to 5.

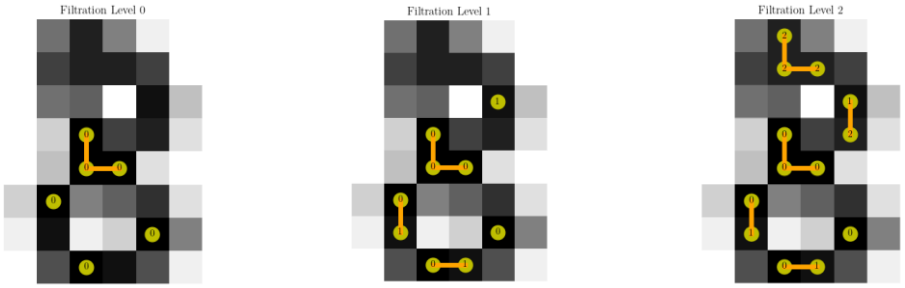

Figure 3. Filtration level 0-2.

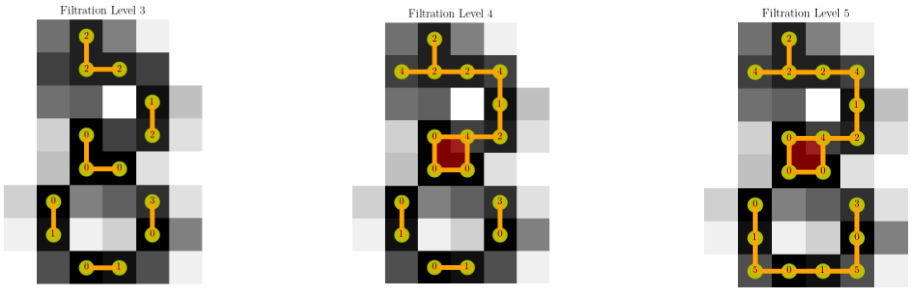

Figure 3. Filtration level 3-5.

The other filtrations were performed in a similar manner. Their results are shown in Fig. 5.

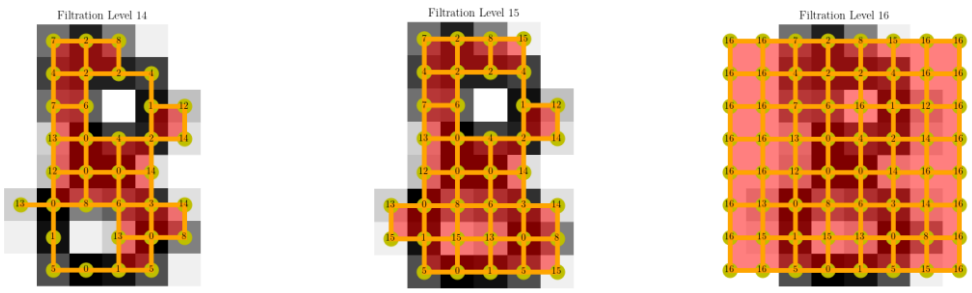

Figure 5. Filtration level 14 -16.

We used the Gudhi Python package to calculate the persistence of the cubical complex constructed using V-construction and displayed the resulting Persistence Diagram and Bar-code (see Fig. 6).

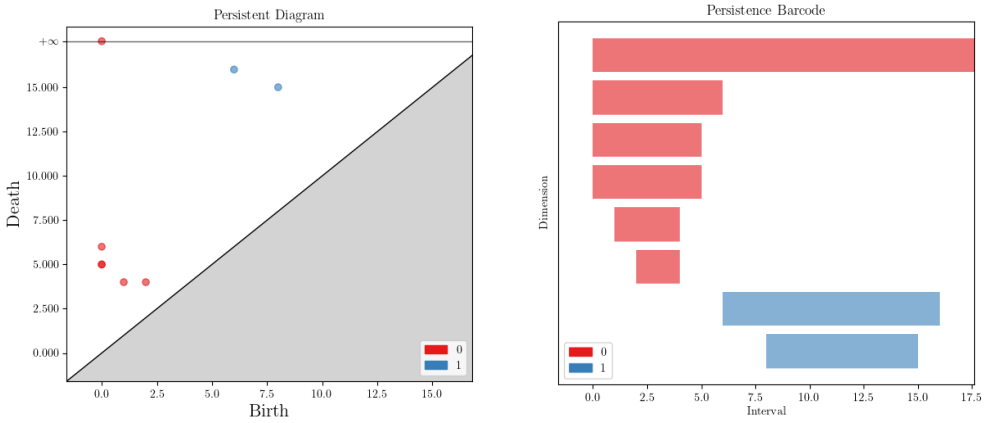

Figure 6. Persistent diagram and barcode of V-construction of digit image 8.

Figs. 7 to 9 provide examples of how the T-construction is generated from an image.

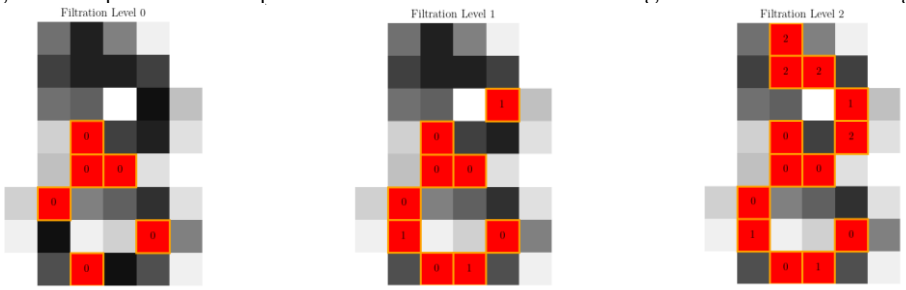

Figure 7. Filtration level 0 -2.

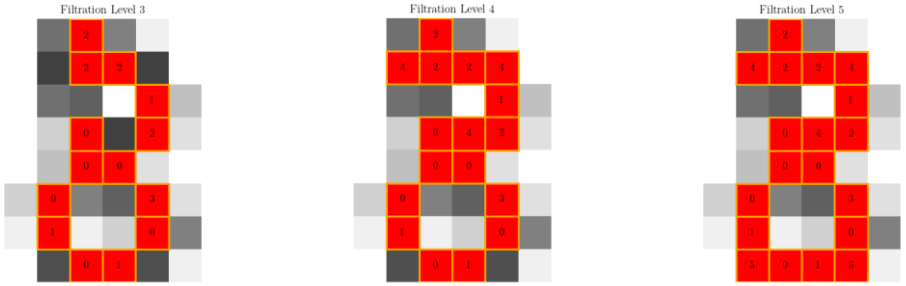

Figure 8. Filtration level 3 - 5.

The remaining filtrations were performed in a similar manner, as depicted in Fig. 9.

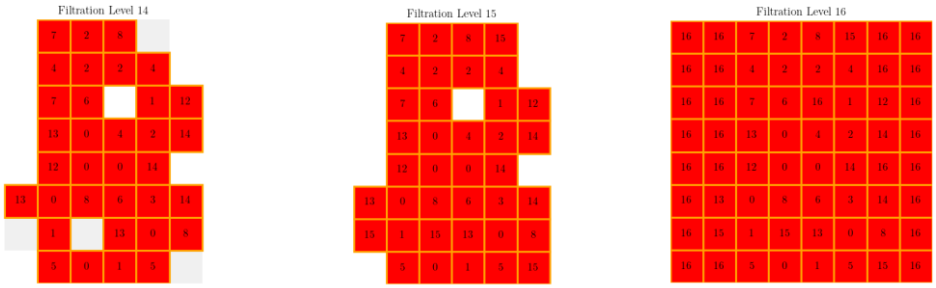

Figure 9. Filtration level 14 - 16.

Then, we calculated the persistence of the cubical complex constructed through T-construction and displayed the corresponding Persistence Diagram and Barcode (see Fig. 10).

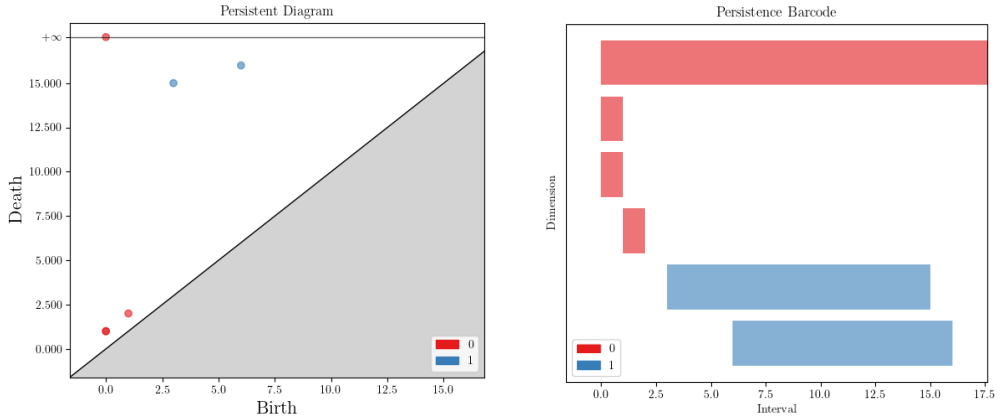

Figure 10. Persistent diagram and barcode of T-construction of digit image 8.

3. Proposed Method

In image denoising using cubical persistent homology, the process begins by representing the image as a cubical complex, where each pixel's intensity serves as its value. We then inverted the pixel values to highlight different features, creating a reversed image. By systematically adjusting the intensity threshold, we generated a series of cubical complexes, each capturing the emergence and disappearance of topological features like edges and textures. These features are visualized in a persistence diagram, where the birth and death of features are plotted. Persistent features, which remain over a wide range of thresholds, are identified as significant, while short-lived ones are considered noise. Focusing on these long-lasting features, we reconstructed the image with reduced noise, ensuring that essential details are preserved. This process effectively differentiates noise and meaningful structures, enhancing the image quality while maintaining its core characteristics. The result is a denoised image that retains important topological features and reduces unnecessary noise, demonstrating the robustness and precision of cubical persistent homology in image processing.

3.1. Finding Actual Significant Topological Features

Our goal is to identify the significant topological features of digit images based on their typical shape. If an image's significant topological features cannot be directly identified (e.g., when black loops are significant), we will reverse the image array by subtracting its grayscale intensity values from 255. This reversed image will then be used to determine the significant topological features. For instance, persistence calculations reveal four loops in the original image of the digit 8, as illustrated in Fig. 11.

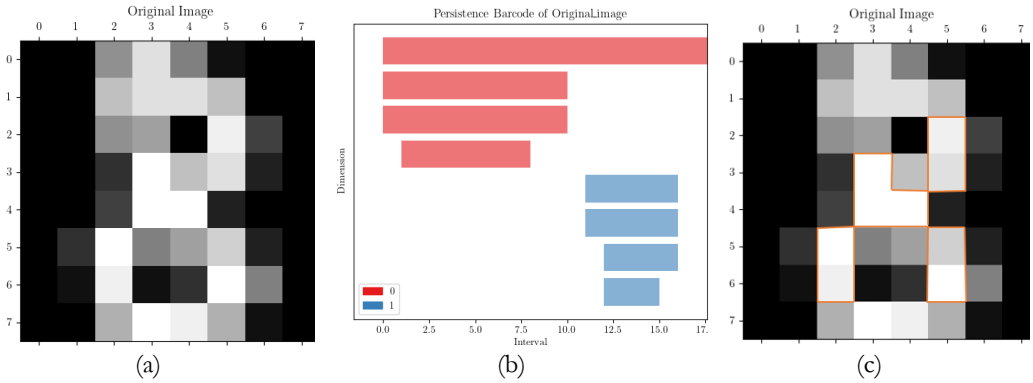

Figure 11. (**a**) Original image; (**b**) its barcode; (**c**) image of digit 8 with wrong features.

To correctly identify the features of the digit 8, we reverse the image array and convert it into a reversed image.

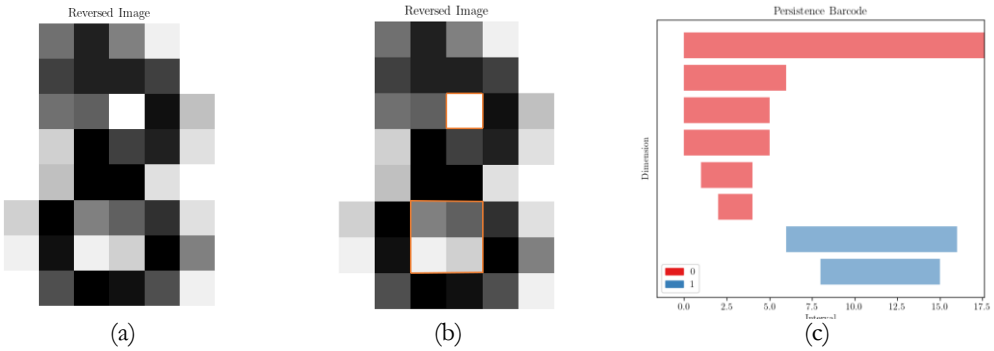

Figure 12. (**a**) Reversed image; (**b**) reversed image with right features; (**c**) its persistent barcode.

From this reversed image, we observe two loops in the correct positions relative to the usual shape of the digit 8, as shown in Fig. 12. In conclusion, if the significant topological features of an image are represented by relatively white pixels, cubical persistent homology can be applied directly to the image. However, suppose the significant features are represented by relatively black pixels. We should reverse the image array by subtracting its grayscale intensity values from 255 before applying cubical persistent homology to find the significant topological features.

3.2. Denoising Image Digits

After computing the cubical persistent homology of digit images, we identify significant topological features such as connected components and loops. Cubical persistent homology enables effective image denoising. At any given filtration level, the image's shape can be observed.

First, we determine the specific filtration level at which the significant topological features are preserved and the usual shape of the image remains intact. We then denoise the image by fixing this filtration level and choosing from the options shown in Fig. 13 for further processing.

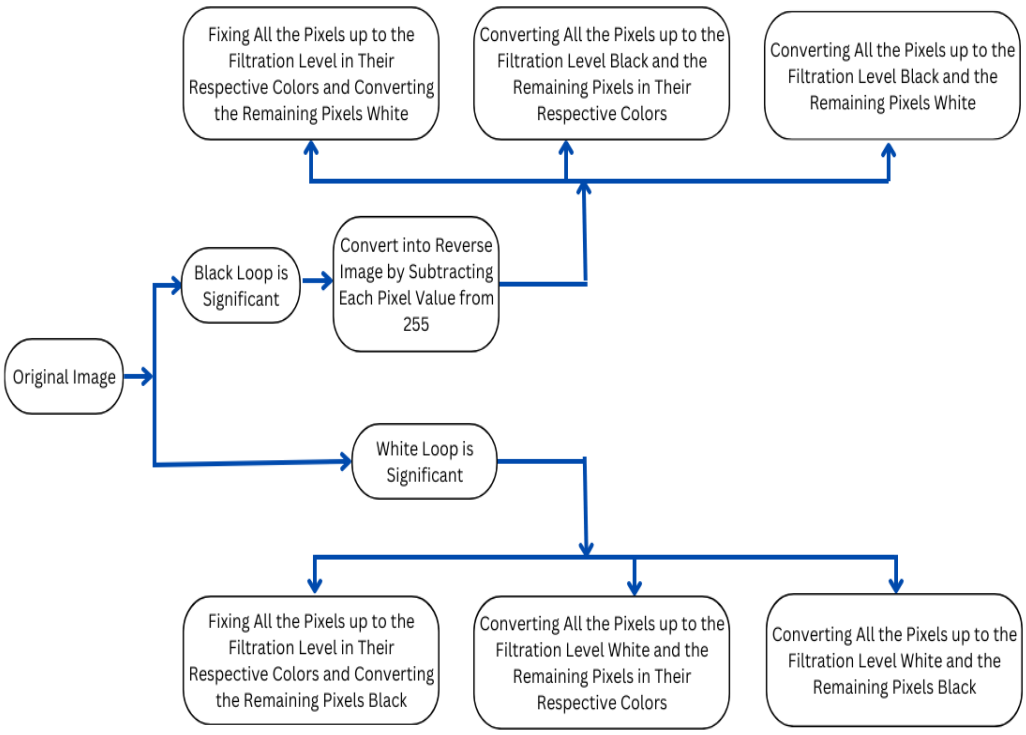

Figure 13. Procedure of denoising an image.

3.3. Algorithm and Theoratical Foundations

Algorithm 1. Selecting Optimal Filtration Level

INPUT: Grayscale Image as an Image Array.
OUTPUT: Optimal filtration level as a set.

1: For each dimension d, compute the lifetimes of topological features $(\text{death} - \text{birth})$ and store these as pairs $(\text{Birth}_i, \text{Death}_i)$.
2: For each dimension d, sort the computed pairs $(\text{Birth}_i, \text{Death}_i)$ in descending order based on their lifetimes (i.e., $\text{Death}_i - \text{Birth}_i$).
3: From the sorted pairs, identify the set of significant topological features S_d for each dimension d.
4: For each identified significant feature $f_i = (\text{Birth}_i, \text{Death}_i) \in S_d$, represent it as a closed-open interval $I_i = [\text{Birth}_i, \text{Death}_i)$.
5: Consider each closed-open interval I_i as a set T_i for each dimension d.
6: Compute the intersection $X_d = \bigcap_{T \in T_d} T$ of all sets T_i corresponding to the significant topological features in each dimension d.
7: If the intersection X_d is empty, then select the interval with the maximum lifetime from the set of significant intervals S_d for each dimension d, and represent it as T_{max_d}.
8: Compute the set difference $Y_d = X_d \setminus \bigcup_{T \in T_d^c} T$, where T_d^c represents the sets of insignificant topological features in each dimension d. If X_d is empty, replace X_d with T_{max_d}.
9: Compute the final intersection $Z = \bigcap_{d=0}^{D} Y_d$ across all dimensions d to obtain the optimal filtration level.

Theorem 1. *Let $\mathcal{F}_d = \{f_i = (Birth_i, Death_i)\}_{i=1}^{n_d}$ be a set of topological features in dimension d. The lifetimes of these features, defined as $Lifetime_i = Death_i - Birth_i$, can be ordered in a non-increasing sequence, resulting in a unique sequence.*

Proof of Theorem 1. Consider each $f_i \in \mathcal{F}_d$ with Birth_i and Death_i such that $0 \leq \text{Birth}_i \leq \text{Death}_i$. The lifetime of f_i is given by: $\text{Lifetime}_i = \text{Death}_i - \text{Birth}_i$
Since Birth_i and Death_i are real numbers with $\text{Birth}_i \leq \text{Death}_i$, it follows that $\text{Lifetime}_i \geq 0$.
Define the ordering relation $\geq$ on $\mathcal{F}_d$ such that for any two features f_i and f_j, we say $f_i \geq f_j$ if and only if $\text{Lifetime}_i \geq \text{Lifetime}_j$. This relation is reflexive, antisymmetric, and transitive, satisfying the properties of a total order. Therefore, the lifetimes can be arranged in a non-increasing sequence: $\text{Lifetime}_1 \geq \text{Lifetime}_2 \geq \cdots \geq \text{Lifetime}_{n_d}$
If $\text{Lifetime}_i = \text{Lifetime}_j$ for some $i \neq j$, the sorting procedure is still well-defined and yields a unique sequence by maintaining the order of appearance or applying secondary sorting criteria.
Thus, the ordering of lifetimes is both well-defined and unique.

Proposition 2. *For each dimension d, the set of significant topological features S_d is non-empty, provided the threshold τ or selection criteria σ_d is appropriately defined.*
Proof of Proposition 2. Let $\mathcal{F}_d$ be the set of topological features in dimension d with lifetimes $\text{Lifetime}_i = \text{Death}_i - \text{Birth}_i$. Define the threshold $\tau \geq 0$ such that: $S_d = \{f_i \in \mathcal{F}_d : \text{Lifetime}_i \geq \tau\}$
Alternatively, let σ_d be a selection criterion that identifies significant features based on persistence or other topological considerations. Define: $S_d = \{f_i \in \mathcal{F}_d : f_i \text{ satisfies } \sigma_d\}$
Since $\mathcal{F}_d$ is non-empty, and τ or σ_d is defined to include at least one feature (e.g., $\tau = 0$ or criteria based on the longest lifetime), it follows that $S_d \subseteq \mathcal{F}_d$ and $S_d \neq \emptyset$.
Thus, S_d is non-empty under appropriately defined conditions.

Theorem 2. *For any significant feature $f_i = (Birth_i, Death_i) \in S_d$, the conversion to the closed-open interval $[Birth_i, Death_i)$ is well-defined.*

Proof of Theorem 2. Let $f_i = (\text{Birth}_i, \text{Death}_i)$ represent a significant topological feature in dimension d, where $\text{Birth}_i, \text{Death}_i \in \mathbb{R}$ with $\text{Birth}_i \leq \text{Death}_i$. Define the closed-open interval: $I_i = [\text{Birth}_i, \text{Death}_i) = \{ t \in \mathbb{R} \mid \text{Birth}_i \leq t < \text{Death}_i \}$.
Existence: Since $\text{Birth}_i \leq \text{Death}_i$, the set I_i is non-empty. The closed-open interval includes all real numbers from Birth_i up to, but not including, Death_i. By definition, there exists at least one real number $t \in [\text{Birth}_i, \text{Death}_i)$, confirming that $I_i \neq \emptyset$.
Well-Defined Nature: The interval I_i is well-defined because it satisfies the properties of a closed-open interval: it contains its left endpoint Birth_i (i.e., $\text{Birth}_i \in I_i$), and does not contain its right endpoint Death_i (i.e., $\text{Death}_i \notin I_i$). This ensures that the feature's start (birth) and end (death) are distinctly represented in the filtration process.
Thus, the conversion of f_i to the interval $[\text{Birth}_i, \text{Death}_i)$ is well-defined.

Proposition 2. *Each interval* $I_i = [Birth_i, Death_i)$ *in* $\mathcal{I}_d$ *can be uniquely represented as a set of integers:* $T_i = \{k \in \mathbb{Z}: Birth_i \leq k < Death_i\}$

Proof of Proposition 2. Consider the closed-open interval $I_i = [\text{Birth}_i, \text{Death}_i)$, where $\text{Birth}_i, \text{Death}_i \in \mathbb{Z}$. Define the corresponding set of integers: $T_i = \{k \in \mathbb{Z}: \text{Birth}_i \leq k < \text{Death}_i\}$
Since T_i consists of all integers between Birth_i (inclusive) and Death_i (exclusive), the set T_i uniquely represents the interval I_i. No two distinct intervals I_i and I_j can produce the same set T_i, ensuring uniqueness.

Thus, the conversion from intervals to sets of integers is both well-defined and unique.

Theorem 3. *Let* $T_d = \{ T_i \mid i \in I_d \}$ *represent the collection of sets corresponding to significant topological features in dimension* d. *If* $X_d = \bigcap_{T \in T_d} T$ *is the intersection of all such sets for dimension* d, *then either:*
1. The intersection $X_d \neq \emptyset$, *or*
2. If the intersection is empty, the interval with the maximum lifetime is chosen as a proxy for the intersection.

Proof of Theorem 3. We begin by considering T_d, the collection of sets corresponding to the significant topological features in dimension d. These sets are derived from closed-open intervals $I_i = [\text{Birth}_i, \text{Death}_i)$, where each I_i represents the persistence of a topological feature in dimension d.
Each $T_i \in T_d$ is derived from the persistence interval $I_i = [\text{Birth}_i, \text{Death}_i)$. By the definition of persistent homology, $\text{Death}_i > \text{Birth}_i$,meaning I_i is a non-empty interval. Since each interval is non-empty, the corresponding set T_i is also non-empty: $T_i \neq \emptyset$ for all $i \in I_d$.
This guarantees that all sets $T_d = \{T_i\}$ are non-empty.
For finite collections of non-empty sets, the intersection is non-empty if a common element exists among them. That is, for all $T_i \in T_d$, if there exists a common filtration level that belongs to each T_i, the intersection: $X_d = \bigcap_{T \in T_d} T$ is non-empty. The set X_d represents the collection of filtration levels where significant topological features in dimension d coexist. If such common filtration levels exist, $X_d \neq \emptyset$.
If the intersection $X_d = \bigcap_{T \in T_d} T$ is empty, it means there are no common filtration levels shared by all significant features in dimension d. In this case, the intersection fails, i.e., $X_d = \emptyset$.
To address this scenario, we select the interval corresponding to the topological feature with the maximum lifetime in dimension d. Let the lifetime of a feature i be $\text{Lifetime}_i = \text{Death}_i - \text{Birth}_i$. Then, we choose the interval $I_{\max} \in T_d$ such that (see Equation (7)).

$$\text{Lifetime}_{\max} = \max_{i \in I_d} (\text{Death}_i - \text{Birth}_i). \tag{7}$$

This ensures that even if no common filtration level exists, the most significant topological feature (i.e., the one that persists for the longest time) is preserved.
Thus, the intersection of significant topological features in dimension d, X_d, is non-empty. If, however, $X_d = \emptyset$, we select the interval with the maximum lifetime as a proxy for the

intersection. This ensures the preservation of the most persistent and important topological feature in dimension d.
Hence, $X_d \neq \emptyset$ or the interval with the maximum lifetime is selected.

Corollary 1. *The set difference* $Y_d = X_d \setminus \bigcup_{T \in T_d^c} T$ *is non-empty for each dimension* d.

Proof of Corollary 1. From Theorem 3, we know that $X_d = \bigcap_{T \in T_d} T \neq \emptyset$.
1. Union of Insignificant Features: Consider the set $\bigcup_{T \in T_d^c} T$, which represents the union of all insignificant feature sets in dimension d. Since these are insignificant, they do not necessarily contain the filtration levels associated with significant features.
2. Set Difference Retains Significant Features: The set difference: $Y_d = X_d \setminus \bigcup_{T \in T_d^c} T$ removes only those elements from X_d that are present in the union of insignificant features. Given that X_d consists entirely of significant filtration levels, and $\bigcup_{T \in T_d^c} T$ contains elements from insignificant features, the set difference Y_d retains some elements from X_d that are not part of insignificant features.
Since X_d is non-empty, and the removal of insignificant levels cannot eliminate all elements from X_d, it follows that $Y_d \neq \emptyset$.

Theorem 4. *The final intersection of the results across all dimension* $Z = \bigcap_{d=0}^{D} Y_d$ *is non-empty.*

Proof of Theorem 4. Let Y_d be the non-empty set derived from the set difference in each dimension d as shown in Corollary 1, so $Y_d \neq \emptyset$ for all $d = 0,1, \dots, D$.
Intersection of Non-Empty Sets Across Dimensions:

The final set Z is defined as: $Z = \bigcap_{d=0}^{D} Y_d$. Since each Y_d is non-empty and represents the set of significant filtration levels in dimension d, their intersection will also be non-empty by the finite intersection property. This is because the elements in Z are precisely those filtration levels that are common to all dimensions, and each Y_d contains significant filtration levels. Thus, $Z \neq \emptyset$.

Proposition 3. *Let* $Z = \{z_1, z_2, \dots, z_m\}$ *be the set of filtration levels obtained from the final intersection in Theorem 4, where* $z_1 < z_2 < \cdots < z_m$. *Then, the minimum filtration level* $z_1 \in Z$ *preserves all significant topological features identified during the filtration process.*

Proof of Proposition 3. Let $\mathcal{F}_j = \left\{ F_i^j = \left[b_i^j, d_i^j \right) \mid i \in I_j \right\}$ be the family of closed-open intervals representing significant topological features in dimension j, where b_i^j and d_i^j denote the birth and death times of the i-th topological feature in dimension j. The set Z is defined as: $Z = \bigcap_{j=0}^{d} \left(\bigcap_{i \in I_j} F_i^j \setminus \bigcup_{i \notin I_j} F_i^j \right)$ where I_j indexes the significant features in dimension j.
Let $z_1 = minZ$. For any $z < z_1$, $z \notin F_i^j$ for at least one $i \in I_j$ and some j, which implies that the corresponding topological feature is not fully captured at level z.
Since Z is formed by intersecting intervals F_i^j where significant features exist, z_1 is the first level where all such features are captured $z_1 = \inf\left(\bigcap_{j=0}^{d} \left(\bigcap_{i \in I_j} F_i^j \setminus \bigcup_{i \notin I_j} F_i^j \right) \right)$
Therefore, selecting z_1 ensures that all significant topological features are preserved.

Corollary 2. *Let* $z_1 = minZ$, *where* Z *is as defined in Proposition 3. Then, using* z_1 *for image denoising preserves all significant topological features while modifying other pixels according to the denoising process.*

Proof of Corollary 2. Let $\mathcal{I} = \{ I(x) \mid x \in D \}$ represent the pixel intensities of the image, where D is the image domain. During the filtration process, each pixel's intensity $I(x)$ determines its inclusion in the cubical complex.

At filtration level z_1, the cubical complex $K(z_1)$ includes precisely those features that correspond to intervals F_i^j from Proposition 3.

For any $z < z_1$, there exists at least one interval F_i^j for some i and j such that $z \notin F_i^j$, implying that not all significant features are included at level z.

The denoising process preserves the intensities $I(x)$ of pixels for which $I(x) \leq z_1$ and modifies the intensities for pixels with $I(x) > z_1$. Since z_1 is the earliest level at which all significant features are captured, the denoising process preserves these features while removing noise.

Thus, using z_1 for denoising ensures the preservation of all significant topological features.

Theorem 5. *The minimum filtration level $z_1 = minZ$ from Proposition 3 is optimal in the sense that it is the earliest level at which all significant topological features are preserved. For any $z > z_1$, the same features are preserved, but for any $z < z_1$, some features will be lost.*

Proof of Theorem 5. Let $z_1 = infZ$, where Z is defined as Equation (8).

$$Z = \bigcap_{j=0}^{d} \left(\bigcap_{i \in I_j} F_i^j \setminus \bigcup_{i \notin I_j} F_i^j \right) \tag{8}$$

with $F_i^j = \left[b_i^j, d_i^j \right)$ as the intervals representing significant topological features in dimension j.

1. Preservation at z_1: For each F_i^j, $z_1 \in F_i^j$, implying that all significant topological features are included at level z_1.

2. No Preservation Below z_1: If $z < z_1$, then $z \notin F_i^j$ for at least one $i \in I_j$ and some j, meaning that not all significant features are captured.

3. Preservation Above z_1: For any $z > z_1$, $z \in F_i^j$ for all $i \in I_j$ and j, hence z includes all significant features, but at a later stage.

Thus, z_1 is the earliest filtration level at which all significant topological features are preserved, making it the optimal choice.

4. Results and Discussion

4.1. Data Sets Preparation

The digit datasets for digits 0 to 9, as depicted in Fig. 14, used in this study are obtained from the Scikit-Learn load_digits function, which is based on the 'Optical Recognition of Handwritten Digits' dataset from the UCI Machine Learning Repository [34]. This dataset consists of 5,620 samples, where each digit is represented as an 8x8 grayscale image, resulting in 64 features per image. The pixel intensity values range from 0 (black) to 16 (white) and are derived by downsampling from an original 32x32 grid. The dataset includes ten classes corresponding to the digits 0 to 9, with 3,823 samples allocated for training and 1,797 samples for testing.

It was processed to determine the minimum filtration level to prepare the dataset for analysis using an algorithm based on cubical persistent homology. This filtration level helps identify the essential topological features of the images while filtering out noise. In the filtration level selection, several variables and parameters are crucial for computing persistence diagrams and identifying significant topological features, as described in Table 2. During denoising, certain variables directly affect how well noise is removed while preserving essential features.

Table 2. Variables Related to Filtration Level Selection and Affecting the Denoising Process in CPHBT

Variable	Description	Determination
Filtration Level	A key threshold in cubical persistent homology represents the scale at which topological features	Determined by analyzing persistence diagrams and applying

Variable	Description	Determination
	(such as connected components and loops) are considered significant.	Algorithm 1 to find the most appropriate threshold.
Threshold (Lifetime)	Represents the minimum persistence (birth-death) a topological feature must have to be considered significant. Features with persistence values below this threshold are considered noise, while features above this threshold are retained.	This threshold is determined empirically based on analysis of persistence diagrams, e.g., features with persistence greater than 3 for dimension 0 and 8 for dimension 1 are retained.
Reversing the Image	Before computing the persistent homology, the image is reversed (i.e., pixel intensities are subtracted from 255), transforming black loops into significant topological features.	This is a fixed step to ensure that black features (such as loops) are treated as topologically significant.
Denoising Threshold	The level at which pixel values are either retained or transformed during the denoising process. Pixels below the selected filtration level are preserved, while those above are converted to white (255).	This is set by selecting the maximum filtration level from the persistence diagram (e.g., 12 in our experiments).

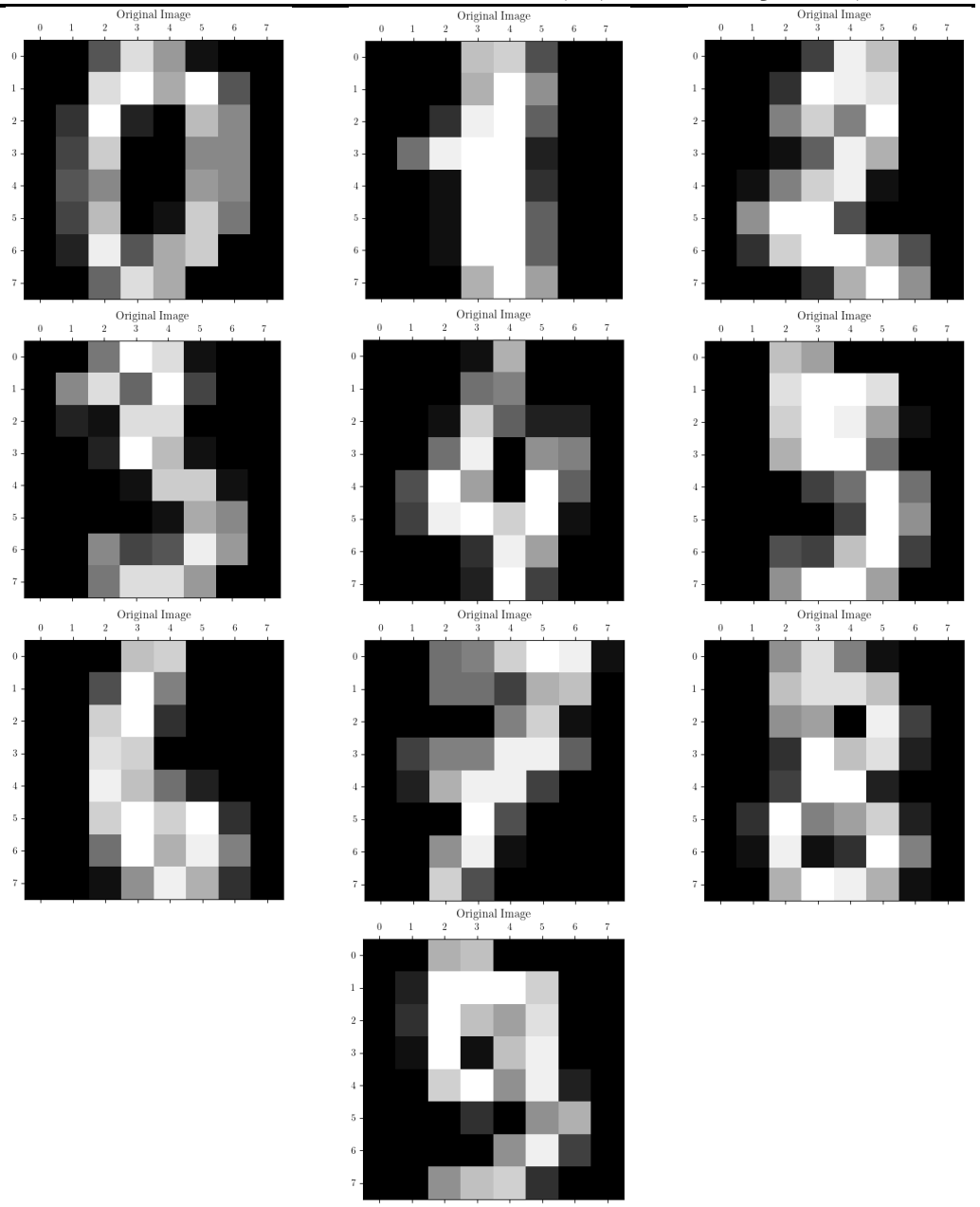

. **Figure 14.** Images of digits 0-9.

4.2. Results and Discussion

In this study, we focus on denoising an image of the digit "8" (refer to Fig. 15(a)). Initially, Gaussian noise was selectively added to pixels with values less than or equal to 3, resulting in what we refer to as the "noisy image" (Fig. 15(b)). To begin the denoising process, we recognized that the black loop structure in the digit "8" is a significant topological feature. Consequently, we transformed the noisy image into its "reversed image" by subtracting each pixel value from 16. Persistent homology was then computed for this reversed image, and its persistence barcode was visualized in Fig. 16.

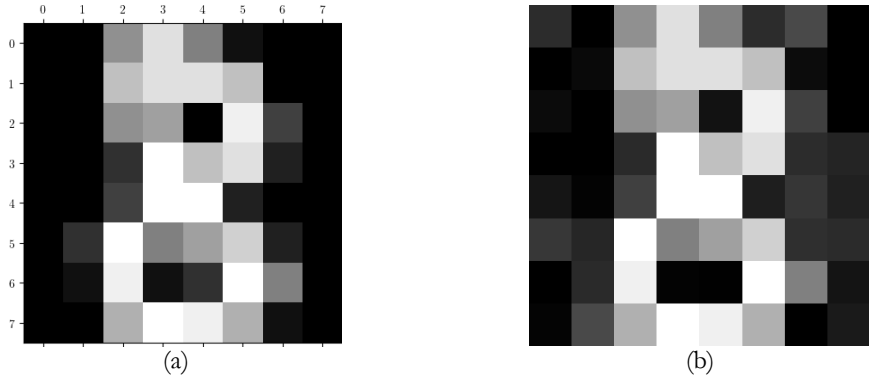

Figure 15. (**a**) Original image of digit 8; (**b**) Noisy image of digit 8

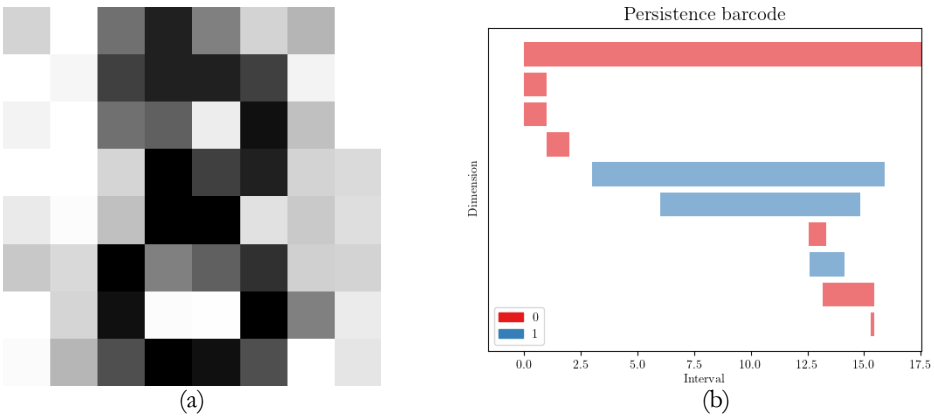

Figure 16. (**a**) Reverse image; (**b**) Its persistent barcode.

Following the persistent homology analysis, we applied Algorithm 1 to determine the optimal filtration level set, which represents the significant topological features:
The Persistence of the complex of reversed image are:
[(1, (3.0, 15.921535410346554)), (1, (6.0, 14.819259943647056)), (1, (12.60644539988603, 14.118956022240548)), (0, (0.0, inf)), (0, (13.188238808415711, 15.426177086436232)), (0, (0.0, 1.0)), (0, (0.0, 1.0)), (0, (1.0, 2.0)), (0, (12.546933661202885, 13.321862582375353)), (0, (15.275028088705957, 15.426177086436232))]
The persistence of the complex (dimension, lifetime, (birth, death)) in descending order of lifetime for each dimension:
Dimension 0:
(0, inf, [0.0, inf)), (0, 2.23793827802052, [13.188238808415711, 15.426177086436232)), (0, 1.0, [0.0, 1.0)), (0, 1.0, [0.0, 1.0)), (0, 1.0, [1.0, 2.0)), (0, 0.7749289211724673, [12.546933661202885, 13.321862582375353)), (0, 0.15114899773027446, [15.275028088705957, 15.426177086436232)).
Dimension 1:
(1, 12.921535410346554, [3.0, 15.921535410346554)), (1, 8.819259943647056, [6.0, 14.819259943647056)), (1, 1.512510622354517, [12.60644539988603, 14.118956022240548)).

The threshold (lifetime) is determined empirically based on analysis of persistence diagrams, e.g., features with persistence greater than 3 for dimension 0 and 8 for dimension 1 are retained. Filtered [birth, death) pairs greater than or equal to the input lifetime value for each dimension:
Dimension 0: [0.0, inf)
Dimension 1: [3.0, 15.921535410346554), [6.0, 14.819259943647056)

These are our expected significant topological features. Filtered [birth, death) pairs less than the input lifetime value for each dimension:
Dimension 0: [13.188238808415711, 15.426177086436232), [0.0, 1.0), [0.0, 1.0), [1.0, 2.0), [12.546933661202885, 13.321862582375353), [15.275028088705957, 15.426177086436232)
Dimension 1: [12.60644539988603, 14.118956022240548)

These are our insignificant topological features.
Then for dimension 0:

$$[0, inf) \setminus \{[13.188238808415711, 15.426177086436232) \cup [0.0, 1.0) \cup [0.0, 1.0) \cup [1.0, 2.0) \cup [12.546933661202885, 13.321862582375353) \cup [15.275028088705957, 15.426177086436232)\}$$
$$= [0, \text{inf})[0,2) \cup [12.546933661202885, 15.426177086436232)$$
$$= [2.0, 12.546933661202885) \cup [15.426177086436232, \text{inf})$$

And for dimension 1:

$$\{[3.0, 15.921535410346554) \cap [6.0, 14.819259943647056)\} \setminus [12.60644539988603, 14.118956022240548)$$
$$= [6.0, 14.819259943647056) \setminus [12.60644539988603, 14.118956022240548)$$
$$= [6.0, 12.60644539988603) \cup [14.118956022240548, 14.819259943647056)$$

And finally,

$$\{[2.0, 12.546933661202885) \cup [15.426177086436232, inf)\} \cap \{[6.0, 12.60644539988603) \cup [14.118956022240548, 14.819259943647056)\}$$
$$= [6.0, 12.546933661202885)$$

We can now select any filtration level from the set [6.0,12.546933661202885). The most suitable maximum filtration level 12 was selected from the filtration level set. All pixel values below or equal to the filtration level were left unchanged to denoise the image, while the remaining pixels were converted to white. This process produced the "filtered reversed image" (see Fig. 17(a)). Afterward, the persistent barcode of the filtered reversed image was analyzed (see Fig. 17(b)).). By reversing the filtered reversed image, we restored its original orientation, generating the "denoised image" (Fig. 17(c)).

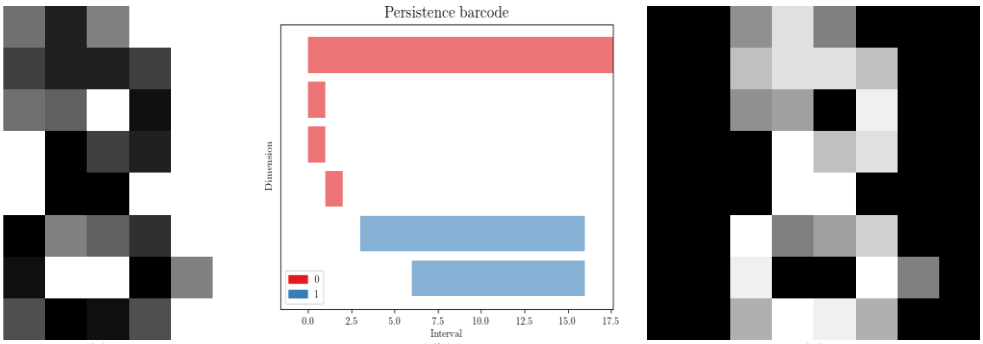

(a) (b) (c)

Figure 17. (**a**) filtered reverse image; (**b**) persistent barcode of filtered reverse image; (**c**) denoised image.

4.2.1. Comparison of Denoising Methods

Next, we applied several standard denoising methods, including Wavelet, Total Variation (TV), and Non-Local Means (NLM), to the noisy image and visualized their respective denoised outputs. Fig. 18 presents the results of various denoising methods. Wavelet denoising (Fig. 18(a)) performed poorly compared to TV (Fig. 18(b)), NLM (Fig. 18(c)), and the CPHBT (Fig. 18(d)). Among these, the denoised image produced by CPHBT is visually superior to the others.

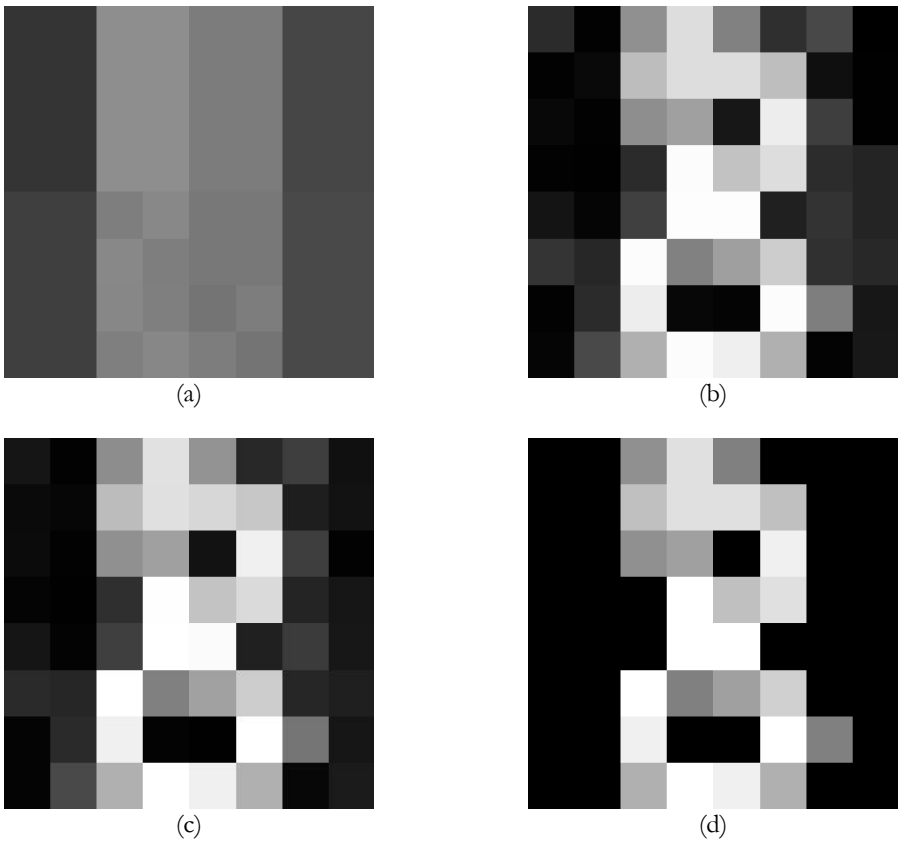

Figure 18. (**a**) Wavelet denoised image; (**b**) TV denoised image; (**c**) NLM denoised image; (**b**) CPHBT denoised image.

4.2.2. Persistent Barcode Analysis

The persistence barcode provides insights into the topological features preserved by each denoising method. Since the black loops are significant in each denoised image, we reversed those images before computing persistent homology to capture and analyze the topological features accurately. The barcode of the Wavelet denoised image shows that a significant loop was mistakenly removed, as illustrated in Fig. 19(a). In contrast, the barcodes for TV and NLM indicate that minor topological noise remains in the images while essential topological features are preserved, as depicted in Fig. 19(b) and Fig. 19(c). However, the CPHBT barcode (see Fig. 19(d)) demonstrates its effectiveness by eliminating minor noise, such as small short-lived loops and small connected components, while preserving the critical topological structures (i.e., a single connected component and two long-lasting loops).

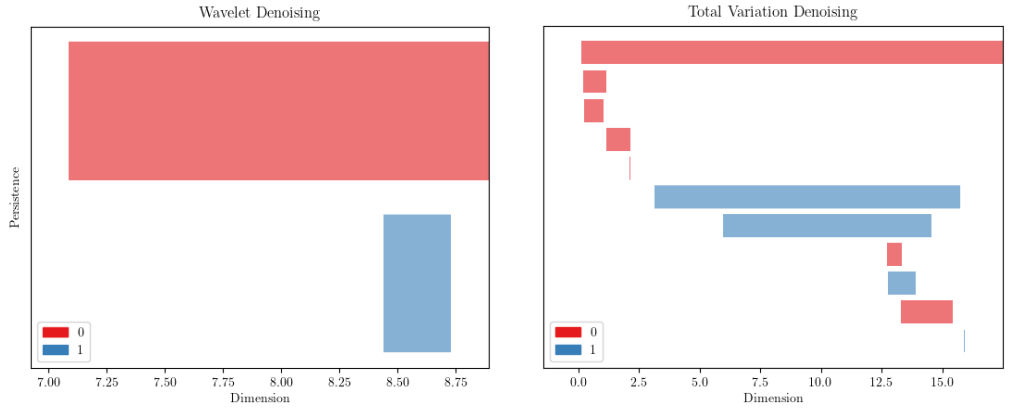

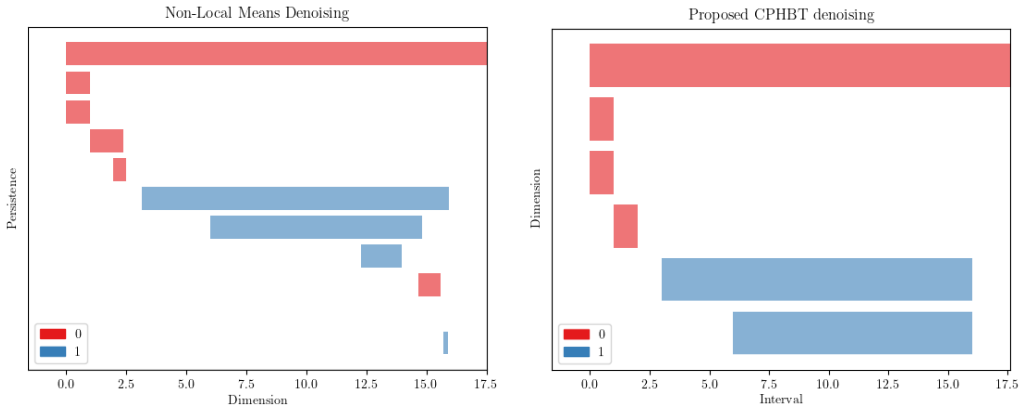

Figure 19. Persistent barcode of (**a**) Wavelet denoised image; (**b**) TV denoised image; (**c**) NLM denoised image; (**b**) CPHBT denoised image.

4.2.3. Quantitative Metrics

We evaluated the denoising methods using the Peak Signal-to-Noise Ratio (PSNR) and Structural Similarity Index Measure (SSIM) by comparing the original image with the denoised outputs, as presented in Table 3.

Table 3. Quantitative Comparison of Denoising Methods.

Method	PSNR	SSIM
Wavelet	10.540533	0.457425
Total Variation	21.522293	0.981153
Non-Local Means	22.092906	0.982235
CPHBT	46.882901	0.990351

As observed in the table, while the SSIM scores for most methods are quite similar, Wavelet denoising underperforms in terms of image quality. Furthermore, the CPHBT method demonstrates superior PSNR and outperforming Wavelet, TV, and NLM.

The primary objective of this ablation study is to determine how the choice of filtration levels influences the preservation of significant topological features and the overall quality of the denoised images. By systematically varying the filtration levels during the denoising process, we can assess the trade-off between noise reduction and the retention of meaningful image structures. We conducted experiments using a range of filtration levels, grouped into the following categories:

- Low Filtration Levels (1-5): These levels capture minimal features.
- Moderate Filtration Levels (6-12): These levels aim to balance noise reduction with preserving significant features.
- High Filtration Levels (13-15): These levels may lead to over-smoothing, potentially eliminating essential details.

For each filtration level, we calculated key evaluation metrics, such as Peak Signal-to-Noise Ratio (PSNR) and Structural Similarity Index Measure (SSIM). We analyzed the corresponding persistent barcodes to identify the preserved topological features.

As seen in Table 4, the ablation study demonstrated that:

- Low Filtration Levels (1-5): These levels failed to preserve many significant topological features, leading to low PSNR and SSIM scores, reflecting poor denoising performance.
- Moderate Filtration Levels (6-12): These levels offered the best trade-off between noise reduction and feature preservation. Notably, the filtration level 12 yielded relatively high PSNR and consistent SSIM scores, indicating that these moderate levels are optimal for denoising.

- High Filtration Levels (13-15): Although these levels reduced noise, they also removed essential details, leading to slightly lower PSNR and SSIM scores than moderate filtration levels.

Table 4. PSNR and SSIM for Different Filtration Levels.

Filtration level	PSNR	SSIM
15	45.500545	0.988865
14	45.634178	0.989086
13	45.835854	0.987911
12	46.882901	0.990351
11	47.475986	0.987884
10	47.475986	0.987884
9	47.475986	0.987884
8	47.475986	0.987884
7	41.961486	0.961314
6	39.902026	0.939693
5	38.240093	0.902840
4	36.826417	0.880955
3	35.077155	0.791092
2	34.547521	0.753172
1	32.693208	0.584335
1	32.693208	0.584335

The persistent barcode analysis (see Fig. 20) also reflects this, with low levels failing to capture key topological features, moderate levels successfully preserving important loops and components while reducing topological noises, and high levels risking the loss of valuable details due to over-smoothing.

This ablation study confirms that the filtration level selection is a critical factor in the effectiveness of our cubical persistent homology-based denoising method. By carefully choosing the filtration level, we can optimize the balance between noise reduction and the preservation of significant topological features, ultimately enhancing the overall quality of the denoised images.

However, despite its effectiveness, the proposed methodology has certain limitations that should be considered. One limitation is the handling of complex image structures. The method may encounter challenges when applied to complex images with intricate noise patterns or where the significant topological features are not easily distinguishable from noise. In such cases, the performance of the denoising process may degrade. Additionally, the accuracy of the denoising process is highly dependent on the resolution and quality of the input images. Images with low resolution or poor contrast may lead to less precise identification of significant topological features, potentially affecting the overall quality of the denoised output. The methodology also involves extensive calculations to determine the lifetimes of topological features and their intersections across multiple dimensions, which can be computationally intensive, particularly for large datasets or high-dimensional data. Furthermore, while the approach demonstrated promising results on handwritten digit images, its generalization to other types of images, especially those with different noise characteristics or more complex structures, requires further validation and refinement.

Figure 20. Persistent barcode of denoised image of digit 8 for filtration level 1-15.

5. Conclusions

In this study, we applied the Cubical Persistent Homology-Based Technique (CPHBT) for denoising images, focusing on the digit "8" from the Optical Recognition of Handwritten Digits dataset. By leveraging the topological insights provided by persistent homology, our approach effectively filtered out noise while preserving essential features, such as black loops, that characterize the digit. When compared to conventional denoising methods like Wavelet, Total Variation (TV), and Non-Local Means (NLM), the CPHBT method demonstrated superior results, achieving the highest PSNR and SSIM scores and producing visually clearer images with preserved key structures.

However, the CPHBT approach also comes with several limitations. First, the computational complexity of persistent homology calculations can be prohibitive, particularly for larger images or real-time applications, where performance is crucial. Second, the method's

sensitivity to filtration level selection can affect the quality of denoising, as choosing the wrong threshold may either leave too much noise or inadvertently remove important features. Third, the approach has been applied to grayscale images, limiting its applicability to broader image types, such as color images or high-resolution datasets, without further adjustments. Lastly, the current method primarily focuses on topological structures, which may not fully account for other image characteristics important in specific domains (e.g., texture or color fidelity).

In future work, improving the computational efficiency of persistent homology algorithms, extending the technique to handle color images, and exploring adaptive methods for automatically determining optimal filtration levels could enhance the scalability and general applicability of the technique across various image denoising tasks.

Author Contributions: Conceptualization, validation, formal analysis: Md. Al-Imran, Mst Zinia Afroz Liza, Md. Morshed Bin Shiraj, Md. Masum Murshed and Nasima Akhter; methodology. Software, resources, writing—original draft preparation, visualization: Md. Al-Imran and Mst Zinia Afroz Liza; investigation: Md. Al-Imran, Mst Zinia Afroz Liza, and Md. Morshed Bin Shiraj; data curation: Md. Al-Imran; writing—review and editing: Md. Morshed Bin Shiraj, Md. Masum Murshed and Nasima Akhter; project administration: Md. Morshed Bin Shiraj and Md. Masum Murshed; supervision: Md. Masum Murshed and Nasima Akhter; funding acquisition: Md. Masum Murshed and Nasima Akhter.

Funding: This study was partially funded by the Ministry of Science and Technology (MoST) of Bangladesh, which awarded fellowships to Md. Al-Imran, Mst Zinia Afroz Liza, and Md. Morshed Bin Shiraj for the 2023–2024 academic year and by the Dean of the Faculty of Science at the University of Rajshahi, through Prof. Dr. Nasima Akhter

Acknowledgments: The authors would like to express their gratitude to the Ministry of Science and Technology (MoST) and the Dean of the Faculty of Science at the University of Rajshahi for their financial support of this research.

Conflicts of Interest: The authors declare no conflict of interest.

References

[1] S. Mallat, *A Wavelet Tour of Signal Processing*. Elsevier, 2009. doi: 10.1016/B978-0-12-374370-1.X0001-8.
[2] L. I. Rudin, S. Osher, and E. Fatemi, "Nonlinear total variation based noise removal algorithms," *Phys. D Nonlinear Phenom.*, vol. 60, no. 1–4, pp. 259–268, Nov. 1992, doi: 10.1016/0167-2789(92)90242-F.
[3] A. Buades, B. Coll, and J.-M. Morel, "A Non-Local Algorithm for Image Denoising," in *2005 IEEE Computer Society Conference on Computer Vision and Pattern Recognition (CVPR'05)*, 2005, vol. 2, pp. 60–65. doi: 10.1109/CVPR.2005.38.
[4] D. L. Donoho and I. M. Johnstone, "Ideal spatial adaptation by wavelet shrinkage," *Biometrika*, vol. 81, no. 3, pp. 425–455, Sep. 1994, doi: 10.1093/biomet/81.3.425.
[5] M. Nikolova, "An Algorithm for Total Variation Minimization and Applications," *J. Math. Imaging Vis.*, vol. 20, no. 1/2, pp. 89–97, Jan. 2004, doi: 10.1023/B:JMIV.0000011321.19549.88.
[6] A. Buades, B. Coll, and J.-M. Morel, "Non-Local Means Denoising," *Image Process. Line*, vol. 1, pp. 208–212, Sep. 2011, doi: 10.5201/ipol.2011.bcm_nlm.
[7] P. K. Rajan, "Two-dimensional digital signal processing II: Transforms and median filters," *Proc. IEEE*, vol. 70, no. 7, pp. 780–781, Jul. 1982, doi: 10.1109/PROC.1982.12396.
[8] J. Mairal, M. Elad, and G. Sapiro, "Sparse Representation for Color Image Restoration," *IEEE Trans. Image Process.*, vol. 17, no. 1, pp. 53–69, Jan. 2008, doi: 10.1109/TIP.2007.911828.
[9] N. Kamalakshi and H. Naganna, "Persistent Homology Residual Learning of Deep Convolution Neural Network for Block Match Three Dimension De-Noising Algorithm," *J. Comput. Theor. Nanosci.*, vol. 17, no. 9, pp. 4340–4343, Jul. 2020, doi: 10.1166/jctn.2020.9073.
[10] A. Malyugina, N. Anantrasirichai, and D. Bull, "A topological loss function for image Denoising on a new BVI-lowlight dataset," *Signal Processing*, vol. 211, p. 109081, Oct. 2023, doi: 10.1016/j.sigpro.2023.109081.
[11] S. Choe and S. Ramanna, "Cubical Homology-Based Machine Learning: An Application in Image Classification," *Axioms*, vol. 11, no. 3, p. 112, Mar. 2022, doi: 10.3390/axioms11030112.
[12] J. Kloke and G. Carlsson, "Topological de-noising: Strengthening the topological signal," *arXiv preprint*. 2009.
[13] Y.-M. Chung, S. Day, and C.-S. Hu, "A multi-parameter persistence framework for mathematical morphology," *Sci. Rep.*, vol. 12, no. 1, p. 6427, Apr. 2022, doi: 10.1038/s41598-022-09464-7.
[14] H. Edelsbrunner and J. L. Harer, *Computational topology: an introduction*. American Mathematical Society, 2022.
[15] N. Otter, M. A. Porter, U. Tillmann, P. Grindrod, and H. A. Harrington, "A roadmap for the computation of persistent homology," *EPJ Data Sci.*, vol. 6, no. 1, p. 17, Dec. 2017, doi: 10.1140/epjds/s13688-017-0109-5.

[16] A. Zomorodian and G. Carlsson, "Computing Persistent Homology," *Discrete Comput. Geom.*, vol. 33, no. 2, pp. 249–274, Feb. 2005, doi: 10.1007/s00454-004-1146-y.
[17] Edelsbrunner, Letscher, and Zomorodian, "Topological Persistence and Simplification," *Discrete Comput. Geom.*, vol. 28, no. 4, pp. 511–533, Nov. 2002, doi: 10.1007/s00454-002-2885-2.
[18] T. Kaczynski, K. M. Mischaikow, and M. Mrozek, *Computational homology*, vol. 157. New York: Springer, 2004.
[19] H. Wagner, C. Chen, and E. Vuçini, "Efficient Computation of Persistent Homology for Cubical Data," in *Mathematics and Visualization*, vol. 0, 2012, pp. 91–106. doi: 10.1007/978-3-642-23175-9_7.
[20] S. Kaji, T. Sudo, and K. Ahara, "Cubical Ripser: Software for computing persistent homology of image and volume data," *arXiv preprint*. May 23, 2020. doi: 10.48550/arXiv.2005.12692.
[21] A. François and R. Tinarrage, "Train-Free Segmentation in MRI with Cubical Persistent Homology," *arXiv preprint*. Jan. 02, 2024. doi: 10.48550/arXiv.2401.01160.
[22] G. Carlsson, "Topology and data," *Bull. Am. Math. Soc.*, vol. 46, no. 2, pp. 255–308, Jan. 2009, doi: 10.1090/S0273-0979-09-01249-X.
[23] P. Frosini and C. Landi, "Persistent Betti numbers for a noise tolerant shape-based approach to image retrieval," *Pattern Recognit. Lett.*, vol. 34, no. 8, pp. 863–872, Jun. 2013, doi: 10.1016/j.patrec.2012.10.015.
[24] P. Bendich, J. S. Marron, E. Miller, A. Pieloch, and S. Skwerer, "Persistent homology analysis of brain artery trees," *Ann. Appl. Stat.*, vol. 10, no. 1, Mar. 2016, doi: 10.1214/15-AOAS886.
[25] H. Adams, A. Tausz, and M. Vejdemo-Johansson, "javaPlex: A Research Software Package for Persistent (Co)Homology," in Lecture Notes in Computer Science (including subseries Lecture Notes in Artificial Intelligence and Lecture Notes in Bioinformatics), vol. 8592 LNCS, 2014, pp. 129–136. doi: 10.1007/978-3-662-44199-2_23.
[26] F. A. Khasawneh and E. Munch, "Chatter detection in turning using persistent homology," *Mech. Syst. Signal Process.*, vol. 70–71, pp. 527–541, Mar. 2016, doi: 10.1016/j.ymssp.2015.09.046.
[27] F. Chazal, V. de Silva, M. Glisse, and S. Oudot, *The Structure and Stability of Persistence Modules*. Cham: Springer International Publishing, 2016. doi: 10.1007/978-3-319-42545-0.
[28] M. Benedetti, J. Realpe-Gómez, R. Biswas, and A. Perdomo-Ortiz, "Quantum-Assisted Learning of Hardware-Embedded Probabilistic Graphical Models," *Phys. Rev. X*, vol. 7, no. 4, p. 041052, Nov. 2017, doi: 10.1103/PhysRevX.7.041052.
[29] B. Bleile, A. Garin, T. Heiss, K. Maggs, and V. Robins, "The Persistent Homology of Dual Digital Image Constructions," in *Association for Women in Mathematics Series*, vol. 30, 2022, pp. 1–26. doi: 10.1007/978-3-030-95519-9_1.
[30] V. Robins, P. J. Wood, and A. P. Sheppard, "Theory and Algorithms for Constructing Discrete Morse Complexes from Grayscale Digital Images," *IEEE Trans. Pattern Anal. Mach. Intell.*, vol. 33, no. 8, pp. 1646–1658, Aug. 2011, doi: 10.1109/TPAMI.2011.95.
[31] S. Tymochko, E. Munch, J. Dunion, K. Corbosiero, and R. Torn, "Using persistent homology to quantify a diurnal cycle in hurricanes," *Pattern Recognit. Lett.*, vol. 133, pp. 137–143, May 2020, doi: 10.1016/j.patrec.2020.02.022.
[32] O. Dunaeva *et al.*, "The classification of endoscopy images with persistent homology," *Pattern Recognit. Lett.*, vol. 83, pp. 13–22, Nov. 2016, doi: 10.1016/j.patrec.2015.12.012.
[33] V. . Kovalevsky, "Finite topology as applied to image analysis," *Comput. Vision, Graph. Image Process.*, vol. 46, no. 2, pp. 141–161, May 1989, doi: 10.1016/0734-189X(89)90165-5.
[34] E. Alpaydin and C. Kaynak, "Optical Recognition of Handwirtten Digits." UCI Machine Learning Repository, 1998. doi: 10.24432/C50P49.